GANIL

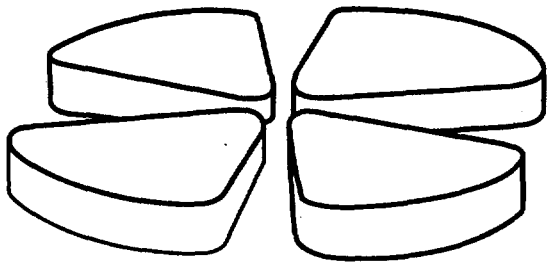

TDHF simulation of the expansion of abraded nuclei.

D. Lacroix[1], Ph. Chomaz[1]
(1)G.A.N.I.L, B.P. 5027, F-14076 Caen Cedex 5, France.

GANIL P 98 09

TDHF simulation of the expansion of abraded nuclei.

D. Lacroix[1], Ph. Chomaz[1]
(1)G.A.N.I.L, B.P. 5027, F-14076 Caen Cedex 5, France.

March 9, 1998

Abstract

A recent interpretation of the caloric curve based on the expansion of the abraded spectator nuclear is re-analysed in the framework of the Time Dependent Hartree Fock (TDHF) evolution. It is shown that the TDHF dynamics can not be reduced to a single monopolar collective motion at moderate energy. The inclusion of other important collective degrees of freedom may lead to the dynamical creation of hollow structure. Then, low density regions could be locally reached after a long time by the creation of these exotic density profiles. The TDHF simulations do not confirm conclusions made when using an monopolar isentropic expansion. In particular the systematic of the minimum density reached during the expansion (the so-called turning points) appears to be different.

PACS: 25.70.-z, 24.10.Cn, 24.10.-i, 25.70.Gh, 24.30.Cz

Keywords: Mean-Field, TDHF, Compound nuclei, Collective motions.

1 Introduction

During the past decade, many works both in experimental and theoretical nuclear physics, have been devoted to the search of the liquid-gas phase transition in Heavy-Ion collisions at intermediate energies. One of the most striking results is the observation of the so-called caloric curve [1]. Indeed, using an isotopic thermometer in conjunction with a measure of the total excitation energy, the authors of ref. [1] have observed that, over a wide range of excitation energy, the temperature of the abraded source seems constant while for a system in an unique phase, one would expect a monotonic increase of the temperature with excitation energy This curve is similar to those known for liquid-gas phase transition at constant pressure. Indeed, in a coexistence region of a single fluid system, it exists a univocal relation between all intensive thermodynamical quantities. From the experimental point of view this curve is actually subject of debates since neither the temperature nor the excitation energy are well defined quantities for small objects in rapid evolution such as hot nuclei[2].

Despite all these difficulties, this observation might be a major step forward since it could be a direct evidence of the liquid-gas phase transition in nuclear matter [3]. Recently, an interpretation of this curve has been proposed by Papp and Nörenberg[4]. Considering the expansion of excited projectile like fragments in a collective model, they predicte that the temperatures at maximum dilution follow approximately the experimental caloric curve. Indeed, the temperature remains almost constant while more and more excited systems are considered because the densities at the turning point of the monopole oscillation rapidely decrease as a the initial excitation increase. As stressed in a recent review article[5], this interpretation is of great importance since, it gives an intuitive connection between the creation of compound nucleus, radial flow, multifragmentation and the final results of Heavy-Ion collisions.

In this paper we would like to re-investigate the same scenario within a microscopic approach: the time dependent Hartree Fock (TDHF) dynamics. Indeed, one may worry about the possible differences between a full quantum treatment and a macroscopic collective model[4].

In the next chapter, we will recall the general framework of the work done in ref.[4]. In part 3, we describe features of the microscopic model we have used. Two forces of Skyrme type are used, one leads to a Soft Equation of State (EOS) in the infinite nuclear matter, the other one to a stiff EOS. These

EOS are key issues when discussing liquid-gas phase transition and in particular mechanical instabilities occurring inside the coexistence zone, namely spinodale instabilities. In this article, we concentrate on the dynamics of expanding systems as predicted by the time dependent Hartree-Fock theory. In order to discuss the observed results we have defined an equivalent of the EOS for finite systems. We have pointed out many differences between the energy of finite-system as a function of the dilution and the infinite nuclear matter case, this could be in part understood in terms of surface effect and coulomb interaction.

We have paid a particular attention in initial conditions, in order to be in same framework as in ref. [4]. The authors of ref. [4] follows the idea of a dominant monopolar collective mode. This idea was used many times in Heavy-Ion Physics at intermediate energy in order to have quantitative informations on how an excited expanding uniform sphere could break[9]. Our calculation do not make this assumption, since we do not impose the domination of one collective mode on the others[12]. In this more general framework, the expansion dynamics appears more complex and is not comparable to the one described in ref. [4]. In particular, for moderate excitation energies (T $<$ 5 MeV) we show that hollow structures can be formed during the TDHF dynamics after several monopolar oscillations. These exotic shapes are obviously not included in simple breathing mode picture[9] and could change considerably our physical understanding of Heavy-Ion collisions at intermediate energy. In a recent work[10], we have shown, that other collective degrees of freedom should be included in order to describe the TDHF expansion. In the following, we will generalize the simple breathing mode picture in order to take into account more collective variables. In particular, we illustrate the inclusion of more accessible density profile by defining a generalized EOS that include hollow density profiles. On the other hand, considering highly excited sources (T $>$ 5 MeV) we observe that the quantum dynamics do not agree with collective models because of the importance of wave propagation and of thermal mixing on the dynamics: barrier transmision, large amplitude motion, lost of collectivity, ...

2 One model for the interpretation of the

caloric curve

Let us first recall the scenario followed by Papp ad Nörenberg in order to understand the ALADIN results concerning the fragmentation of a gold projectile after its interaction with a gold target at 600 MeV/A incident energy[1, 4]. Since the experiment is observing the decay of the projectile-like fragments in peripheral heavy ion reactions, the initial conditions are provided by the abrasion-ablation model[11]: after collision, the projectile of mass A has lost ΔA_i nucleons; the initial excitation $E_i^\star$ of the nucleus is assumed to be related to ΔA_i by

$$E_i^\star = \alpha \Delta A_i \tag{1}$$

In the following simulations, ΔA_i varies from 8 to 108 nucleons and $\alpha = 13.3 MeV$. Temperatures are adjusted in order to get the excitation energies $E_i^\star$ (1) for a spherical nucleus of mass A-ΔA_i The initial density is taken to be lower than the normal density, $\rho_i = 0.8\ \rho_0$ because the abrasion-ablation dynamics is assumed to induce a small dilution through the ejection of few nucleons[4].

Then, authors of ref.[4] follow the expansion of the system as an isentropic self-similar monopole motion: the breathing mode. However, the energy and the entropy slightly evolve in time in order to account for particles evaporation.

Studying the evolution of different such systems with various initial masses, they have shown that, choosing a soft equation of state, the caloric curve could in be explained as the temperature of the emitting source at the turning points of the collective expansion associated with various initial masses and excitation energies. They have also found that using a stiff equation of states reduces the amplitude of the considered monopole vibration leading to different conclusions.

The aim of our paper, is to examine these conclusions within microscopic model known to describe collective dynamics as well as single particle behaviors in a quantum framework: the TDHF approach. In particular, we will test the validity of the breathing mode scenario by comparison with the complete TDHF dynamics.

3 TDHF simulations

3.1 Mean-field approximation

We consider the evolution of hot diluted spherical nuclei in the framework of mean-field theory. The simulation of the desexcitations of excited compressed spherical nuclei is already reported in the literature[13] for nuclei initialized using a Constrained Hartree Fock method (CHF). We use a scaling assumptions in order to prepare the initial nucleus because this method allows to study a broad range of initial dilutions. In the cases where both methods are tractable, we have controled that it gives results comparable with those of CHF [6].

We consider systems saturated in spin and isospin. Nucleons are moving independently in an average spherically-symmetric potential. We use the following parametrization for the effective mean-field potential

$$U[\rho] = \frac{3}{4}\, t_0\, \rho + \frac{(\sigma+2)}{16}\, t_3\, \rho^{\sigma+1} + c\, \nabla^2\rho + V_C. \tag{2}$$

where the surface term, $c\,\nabla^2\rho$, can be related to the usual Skyrme parameters by

$$c = \frac{5t_2 - 3t_1}{16} \tag{3}$$

For sake of simplicity we have taken forces with effective masses equal to the bare one. In order to reduce the numerical instabilities we have used the standard method which consists in replacing the surface term of potential (2) by a folding product with a finite range function [14, 16]

$$U[\rho] = \frac{3}{4}t'_0\, \rho + \frac{(\sigma+2)}{16}t_3\, \rho^{\sigma+1} + V_0\, Y \otimes \rho + V_C \tag{4}$$

where Y is a Yukawa folding function

$$Y(\vec{r}) = \frac{\exp\left(-\frac{r}{a}\right)}{\frac{r}{a}} \tag{5}$$

at the lowest order in the range a this expression is equivalent to the usual Skyrme functional provided that

$$t'_0 = t_0 - \frac{16}{3}\pi a^3 V_0 \tag{6}$$

and that coefficients in the Yukawa folding functions are related by

$$V_0 = \frac{(5t_2 - 3t_1)}{64\pi a^5} = \frac{c}{4\pi a^5} \tag{7}$$

Finally, the direct coulomb potential V_C is introduced in an approximative way by giving an effective charge of $+\frac{Z}{A}$ to each nucleon. Using this potential and a spherically symmetric density, each single-particle wave function can be separated into its radial, angular and spin-isospin part

$$\Phi_\alpha(\vec{r}, \sigma, \tau) = \frac{R_{nl}(r)}{r} Y_{lm}(\theta, \varphi)\chi_s(\sigma)\chi_t(\tau) \tag{8}$$

where α represents all quantum number $\alpha = (n, l, m, s, t)$, in which n is the energy principal number, (l, m) are the usual angular-momentum quantum numbers and (s, t) is the quantization of spin and isospin. If we consider initially a hot system, at temperature T, occupation numbers of various orbitals α are given by a Fermi-Dirac distribution

$$n_{nl} = \frac{1}{\exp\left(\frac{\varepsilon_{nl} - \mu}{T}\right) + 1} \tag{9}$$

where the chemical potential is computed in order to get the correct number of particles. To be able to define particle orbitals at high temperature, a small external field λr^2 has been added to the potential ($\lambda = 0.25$ MeV/fm^2). Finally, the density of our spherical nucleus takes the particular form

$$\rho(r, t) = 4 \sum_{n,l} (2l + 1) n_{nl} \frac{|R_{nl}(r, t)|^2}{4\pi r^2}, \tag{10}$$

Before getting into details of the simulations, we will give some more details about these forces and about the associated Equation Of State (EOS).

3.2 Forces and infinite nuclear matter properties

Following [4], we consider two parametrizations of the potential (4) equivalent to the $SIII$ and the SkM^* forces ([15]). These two forces correspond respectively to a HARD and a SOFT EOS.

Starting with the mean-field potential (2), the total energy per nucleon in the infinite, uniform, spin and isospin saturated nuclear matter is

$$\frac{E}{A} = \frac{E_k}{A} + \frac{3}{8} t_0 \rho_0 + \frac{1}{16} t_3 \rho_0^{(\sigma+1)} \tag{11}$$

where we have introduced the kinetic energy per nucleons $\frac{E_k}{A}$; for a cold gas of fermions this energy can be easily related to the density by

$$\frac{E_k}{A} = \frac{3}{5}\left(\frac{\hbar^2}{2m}\right)\left(\frac{3\pi^2}{2}\rho_0\right)^{\frac{2}{3}} \tag{12}$$

Therefore, the saturation density, ρ_0, is solution of

$$\rho_0\left(\frac{\partial\frac{E}{A}}{\partial\rho}\right)_{\rho=\rho_0} = 0 = \frac{2}{3}\frac{E_k}{A} + \frac{3}{8}t_0\rho_0 + \frac{(\sigma+1)}{16}t_3\rho_0^{(\sigma+1)} \tag{13}$$

which is nothing but the annulation of the pressure at the saturation point (at zero temperature). The infinite nuclear matter incompressibility K_∞ is then given by

$$K_\infty = 9\rho_0^2\left(\frac{\partial^2\frac{E}{A}}{\partial\rho^2}\right)_{\rho=\rho_0} = -2\frac{E_k}{A} + \frac{9\sigma(\sigma+1)}{16}t_3\rho_0^{(1+\sigma)} \tag{14}$$

These three relations (11), (13) and (14) provide an univocal relation between the saturation point properties ρ_0, $\frac{E}{A}$ and K_∞ and the force parameters t_0, t_3 and σ. The parameter c does not influence the infinite uniform medium properties.

If we compute the EOS associated with the parametrization (4) we get similar expressions provided that we use the relation (6): $t_0 = t'_0 + \frac{16}{3}\pi a^3 V_0$. The parameter V_0 and a are related through the relation (7) but are not directly constrained by the EOS. However, for a finite system the relation between (2) and (4) is only valid at the lowest order in a. Therefore, this parameter should remains small. Following ref. [16] we have fixed a to $0.45979fm$. Parameters values leading to same properties as $SIII$ and SkM^* for our parametrization are shown in table 1.

As an illustration, we have plotted the various isentropic EOS in infinite nuclear matter in figure 1 (Top). We have also plotted the isentropic and the isothermal spinodal regions defined as the region where the derivative of the pressure versus the density at constant entropy or temperature is negative. Therefore, in these regions the matter is mechanically unstable against density fluctuations: these are the so-called spinodal instabilities which might be responsible for the fragmentation of the system.

Let us now come to the simulation of finite systems. These numerical simulations consist in two distinct parts: the first one is the initialization of abraded nuclei and the second one the TDHF dynamics.

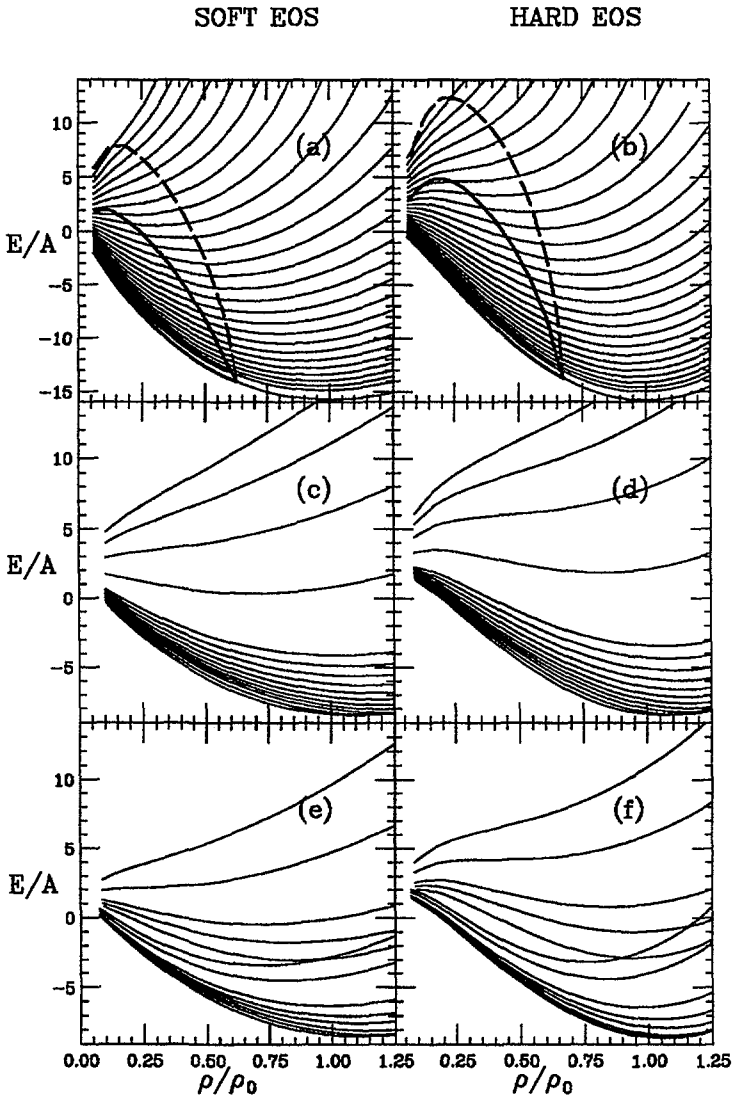

Figure 1: Relations between the energy per nucleon and the central density. Top parts correspond to the infinit medium EOS, each curve is drawn at constant entropy and the entropy variation between two adjacent curves is $\Delta S/k_B = 1$. In such a case both the isothermal (dashed) and the isentropic (solid) spinodal are displayed as thick lines. Middle part corresponds to a $^{197}_{79}$Au nucleus while the bottom part is associated with the various systems considered for the evolution. In the bottom part, curves correspond to decreasing masses (equivalently to increasing excitation energy) from bottom to top of the graphic. More detail is given in the text for the determination of this picture in finite nuclei. For all graphs, left and right part correspond respectively to a soft and a hard EOS.

	Soft EOS (SkM^*)	Hard EOS ($SIII$)
$\frac{E}{A}$ (MeV)	-15.77	-15.85
σ	$\frac{1}{6}$	1
ρ_0 (fm^{-3})	0.16	0.145
t_0 (MeV fm^3)	-2191.73	-435.41
t_3 (MeV fm$^{3(1+\sigma)}$)	18818.8	17258.8
a (fm)	0.45979	0.45979
V_0 (MeV)	-461.07	-401.77
K_∞ (MeV)	198.88	368.4

Table 1: Parameters and properties of the two interactions used in this article.

3.3 Initialization of finite systems

The first step is to initialize our system according to the equation (1). The method used in order to generate a hot and diluted initial source proceeds as follow:

- First we look for the ground state of the nucleus with $A_i = A - \Delta A_i$ nucleons. To do so we use the imaginary time method with a small constraint λr^2 added to the mean field in order to get occupied states, $|\Phi_h\rangle$ (h for hole states), the associated one-body density $\rho = \sum_h |\Phi_h\rangle\, n_h\, \langle\Phi_h|$ where the occupation number are given by equation (9) at zero temperature. Diagonalizing the Shrödinger equation

$$\left\{\frac{-\hbar^2}{2m}\frac{d}{dr^2} + \frac{\hbar^2 l(l+1)}{2mr^2} + U(\rho(r)) + \lambda r^2\right\} R_{nl}(r) = \varepsilon_{nl} R_{nl}(r) \qquad (15)$$

  we can define the single particle states (nl). The small constraint λr^2 insures a limited number of orbitals for treating the continuum. In analogy with the nuclear matter, we define the saturation density, $\rho_0\,(A_i)$, as the central averaged density in a sphere of $2fm$.

- Then, single particle states are occupied according to a Fermi-Dirac statistic (9) using a temperature T as a free parameter. This temperature is defined iteratively in such a way that after the scaling described below, we get the excitation energy defined by Eq. (1)[1]. The chemical

[1]For each ΔA_i, we can define the excitation energy by subtracting the ground state energy of a cold nucleus of size $A-\Delta A_i$ to the energy of the excited nucleus after rescaling.

potential is determined requiring that the total number of particle is $A - \Delta A_i$. The initial entropy of the system is defined by

$$S = -4 \sum_{nl} (2l+1) \left(n_{nl} \log n_{nl} + (1 - n_{nl}) \log(1 - n_{nl}) \right) \qquad (17)$$

- Finally we apply a scaling to each radial wave functions

$$R_{nl}^{new}(r) = \mathcal{N} R_{nl}(\frac{r}{\alpha}) \qquad (18)$$

where $\mathcal{N}$ is a normalization factor. Then we compute the average density $\rho(A_i)$ at the center of the nucleus (within a sphere of 2 fm) and we fixe α in order to get the desired dilatation factor $\eta = \frac{\rho(A_i)}{\rho_0(A_i)} = 0.8$.

After the initialization step we are following an ensemble of diluted nuclei with mass $A - \Delta A_i$ and corresponding excitation energy $E_i^\star$. Each one is associated with an initial entropy S_i. A sample of various initial conditions are given in table 2.

Figure 2 presents various density profiles. On this graph one can spot only minor differences between the two forces.

In order to get a deeper insight in the properties of finite systems, we have plotted the energy of the considered nuclei as a function of their central density: $E = f(\eta)$ (fig.(1) middle and bottom). Each curve is obtained by scaling the wave-functions at fixed occupation numbers (which means that along these curves $S = cte$).[2] Middle part of fig. (1) corresponds to a $^{197}_{79}$Au for various entropies whereas bottom corresponds to masses and entropies reported in table 2.

These curves can be compared to the infinite medium EOS shown in figure 1 (Top). As far as the dynamics is concerned, these isentropic curves have only a meaning if the time dependent density profiles could be obtained one

---

For all these calculations, we have used the expression of the energy corresponding to the potential (4)

$$E = E_{kin} + \int \left\{ \frac{3}{8} t_0 \rho(\vec{r})^2 + \frac{1}{16} t_3 \rho(\vec{r})^{(\sigma+2)} + \frac{V_0}{2} \int Y(r - r') \rho(r) \rho(r') d\vec{r'} \right\} d\vec{r} + E_C \quad (16)$$

In this expression, E_{kin} and E_C are respectively the kinetic and Coulomb energy.

[2]These relations between E , η and S can be considered as a finite system equation of states.

A_i	S_i Soft EOS (SkM^*)	S_i Hard EOS ($SIII$)
191	0.44	0.37
187	0.38	0.35
183	0.45	0.51
177	0.63	0.51
172	0.79	0.71
165	0.97	0.92
158	1.14	1.12
150	1.33	1.31
142	1.52	1.50
134	1.59	1.55
120	1.80	1.82
111	2.0	2.06
98	2.46	2.49
89	2.79	2.80

Table 2: Examples of initial conditions considered. For each initial masses and for the two considered forces, initial entropies are given.

A_i	$\rho_0(A_i)$ Soft EOS (SkM^*)	$\rho_0(A_i)$ Hard EOS ($SIII$)
191	0.142	0.139
187	0.142	0.139
183	0.143	0.140
177	0.147	0.142
172	0.150	0.144
165	0.155	0.147
158	0.160	0.150
150	0.165	0.153
142	0.170	0.157
134	0.155	0.145
120	0.143	0.140
111	0.143	0.140
98	0.154	0.148
89	0.163	0.154

Table 3: Saturation densities for the various initial masses.

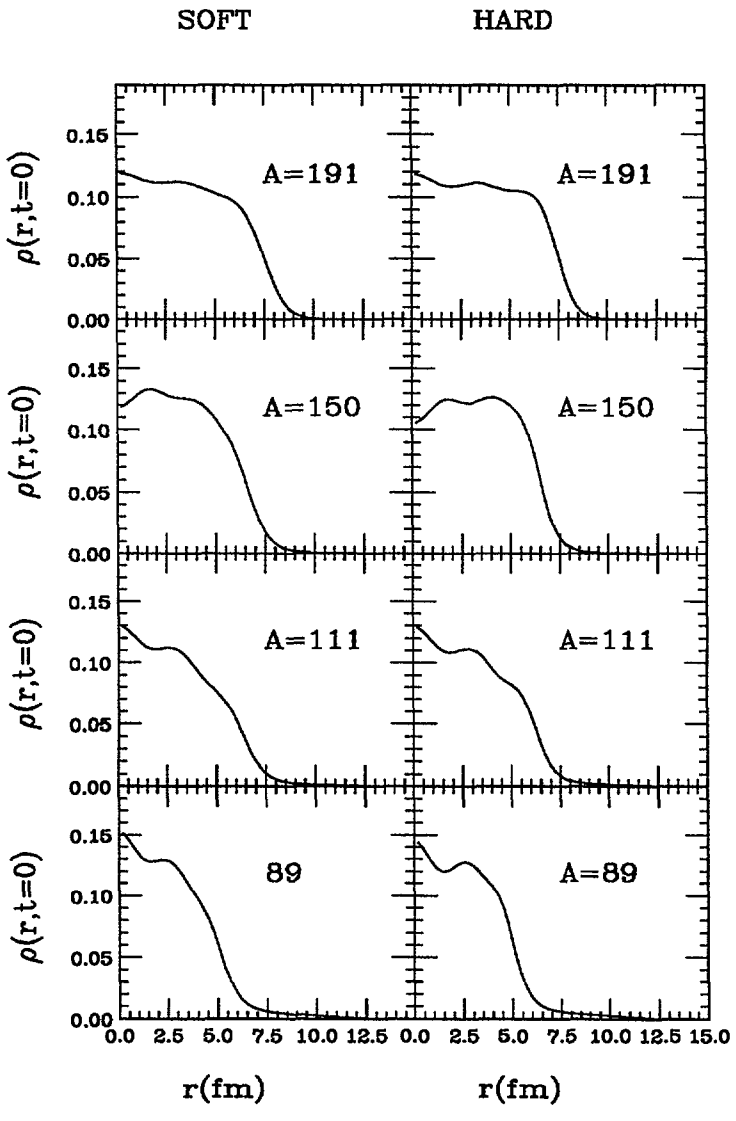

Figure 2: Typical examples of initial density profiles for various initial masses: Left (soft EOS) and right (Hard EOS).

from another by a simple scaling in r-space. This is equivalent to consider the breathing mode as dominant and to neglect other fluctuations in density.

Figure 1 illustrates the fact that finite systems have surface and Coulomb contributions to their energy. This modifies the saturation energy to 8-9 MeV (depending upon the mass of the nucleus considered) instead of 16 MeV found in the case of a neutral infinite system. Moreover, it changes the curvature of the isentropes i.e. it changes the effective compressibility modulus. However, this compressibility remains the main difference between the two ensembles of calculations associated with the two different forces. These isentropes will help us in the understanding of the dynamical evolutions since, in a naive picture, the collective vibration should oscillate around the minimum of the energy for the considered entropy and the turning points of the breathing mode should be simply obtained by requiring energy conservation [3].

3.4 TDHF evolution

Having defined the initial conditions as a given nucleus of size $A_i = A - \Delta A_i$, a given excitation energy and the dilatation coefficient $\eta = 0.8$, we let the system evolve through the TDHF equations [4]

$$i\hbar \frac{\partial R_{nl}(r,t)}{\partial t} = \left\{ \frac{-\hbar^2}{2m} \frac{\partial}{\partial r^2} + \frac{\hbar^2 l(l+1)}{2mr^2} + U\left[\rho\right](r,t) \right\} R_{nl}(r,t) \qquad (19)$$

The potential term $U[\rho]$ is the same as in equation (4). The TDHF equations have the particularity to conserve occupation numbers (n_{nl}) of single particle levels.

$$\frac{d}{dt} n_{nl} = 0 \qquad (20)$$

The entropy of the whole system (17) is thus conserved during the evolution. On the other hand the total energy of the system is also conserved. However, during the evolution, nuclei are evaporating particles and a tail at large distance will develop for the various wave functions R_{nl}. We can try to

[3] Note that, picture (1) depends upon the size of the sphere we have taken in order to define the density (here r=2 fm). This will be discussed in the following.

[4] For the evolution, we have taken a step of time $\Delta t = 0.75 fm/c$. We have discretize the r-space in step of size $\Delta r = 0.2 fm$, the total size of the r-space being 300 fm, this size is big enough to avoid bouncing of evaporated particles against boundaries.

investigate this process using the methods developed in [18] which consist in spliting the r-space into two parts :

- a sphere containing the initial nucleus, here we have considered a sphere of radius 15 fm. This part of the system will be called the nucleus in the rest of this article.
- the rest of the space which will be considered as evaporated particles[5].

Therefore, due to the particle evaporation, the nucleus is continuously loosing mass, energy and entropy [6]. We are thus in the same framework as in ref.[4, 19] but with a microscopic model. The approach we are using is neglecting the collision term because in a self-similar expansion, the gain and the loss term due to collisions are expected to cancel, so that the mean field dominates the dynamics.

4 Discussion of the expansion dynamics

4.1 Evolution of global quantities: evaporation and monopole expansion

In this section, we study the evolution of the various considered nuclei. In fig.(3), we have plotted the evolution of masses and entropies of the systems reported in table 2. All these quantities are computed within a sphere of 15 fm. From this picture we can see that the smaller are the initial masses, the larger are the energies and entropies and so are the number of evaporated particles. Indeed, one can observe that the evaporation is stronger for light highly excited systems with a rapid decrease of the mass and the entropy. However, since in our approach the evaporation is treated as a quantum transmission above or below a potential well the particle evaporation appears rather slow.

[5] We are considering very large space in order to avoid the reflections of the wave packets on the boundaries of the considered r-space.

[6] In general at very low excitation energy the nucleus can even gain entropy because of the dissipation of the collective motion.

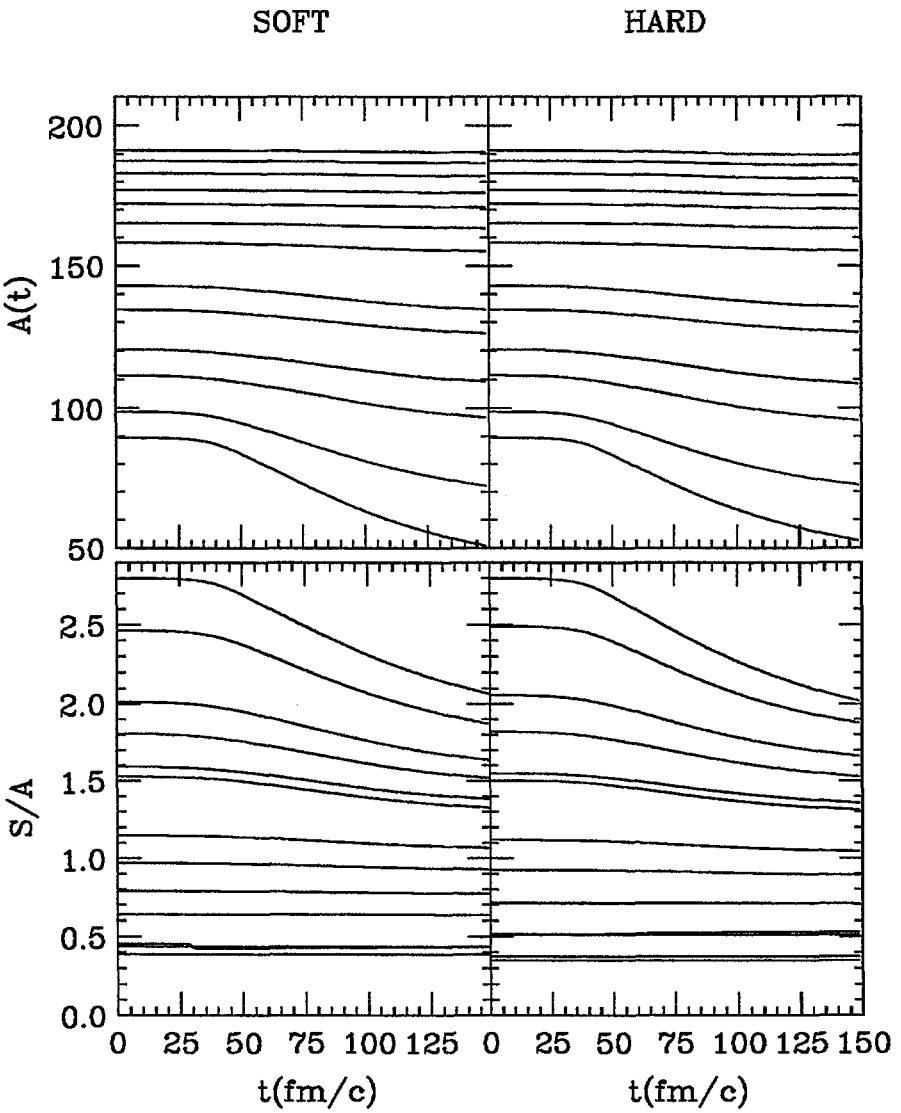

Figure 3: Typical examples of time evolution of the mass, and entropy for the various initial masses considered.

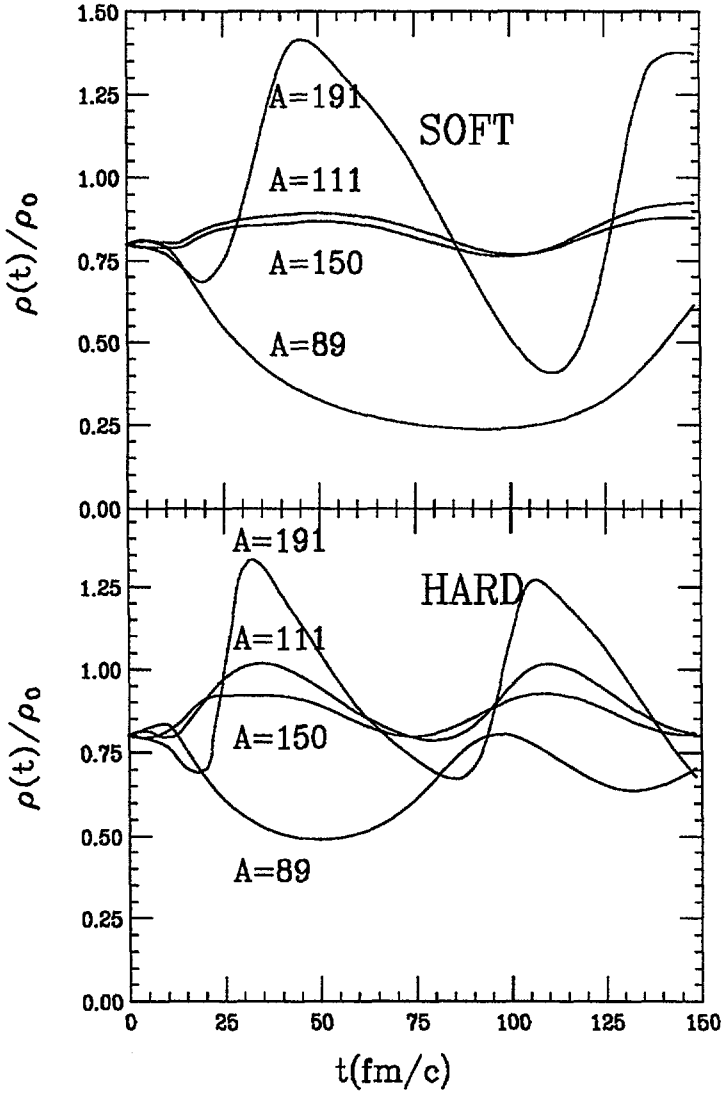

Figure 4: Typical examples of the time evolution of the central density for various initial masses ($A = 191, 150, 111$ and 89.4).

	Soft EOS (SkM^*)		Hard EOS ($SIII$)	
A_i	$\rho_{\min}$ schem	$\rho_{\min}$ exact	$\rho_{\min}$ schem	$\rho_{\min}$ exact
191	0.114	0.058	0.111	0.093
150	0.132	0.126	0.123	0.122
111	0.114	0.110	0.112	0.110
89	0.	0.039	0.	0.076

Table 4: Comparison between the turning point (observed dynamically) and those predicted using a schematic self-similar isentropic dynamics at constant energy.

This monopole motion can be clearly seen in figure 4 which displays the time evolution of the central densities for different initial conditions. From this figure, as expected, collective motion is slower and presents a larger amplitude motion in the case of a soft EOS.

4.2 Discussion of the Collective dynamics

In these figures, we do not observe the fast expansion towards low density regions as reported in reference [4]. Indeed, at moderate energies ($T <$ 5 MeV), we observe that the first minimum (i.e. the first turning point) appears to be close from the initial dilution (see for example $A = 191$). At low excitation energies, the small dilution of the abrasion-ablation stage is followed by a recompression phase. Then, when the system expands again, the averaged density may reach values lower than the initial one.

Conversely, in a simple description assuming a collective dynamics at almost constant entropy and mass, this behavior should be normally understood considering the energetics of isentropes as shown in figure 1. Indeed, schematically, if the system is initially with an excitation energy, E_0, and an entropy, S_0, it will expand or contract till it has reached the other point of the isentrope $S = S_0$ which cut a horizontal line corresponding to the energy $E = E_0$. This schematic procedure is illustrated in figure 6. Values of turning points obtained with this simple construction are compared to those extracted from the simulation in table 4.

For $A = 150$ and $A = 111$, one can see only little differences between results of the schematic construction and those of the exact dynamics. However, they are completely different for $A = 191$ and $A = 89$. Considering

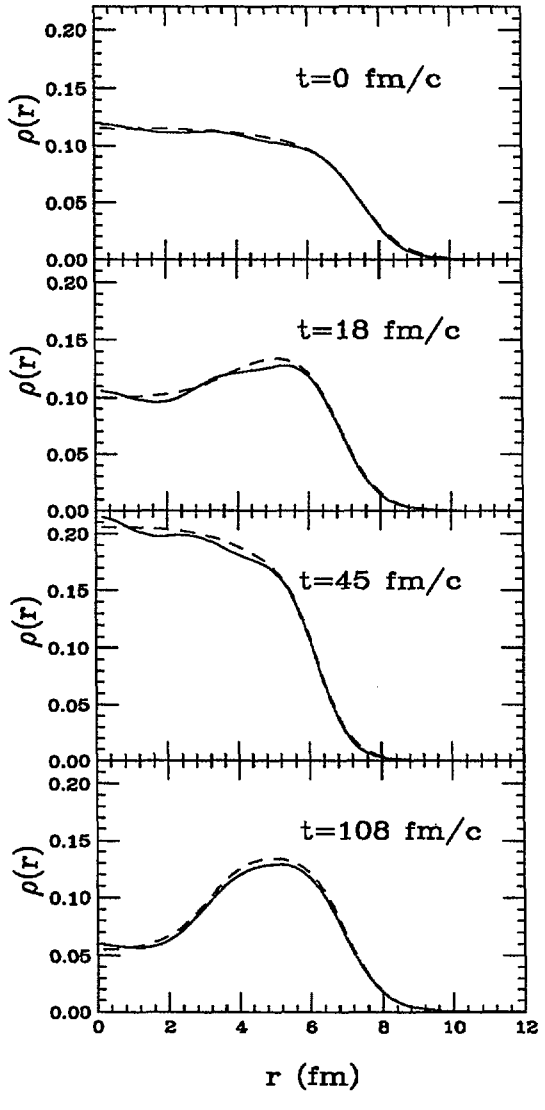

Figure 5: Density profiles taken when the central density reaches its extrema. Figures corresponds to an initial mass $A = 191$ and time $t = 0, 18, 45$ and $108 fm/c$ from top to bottom, which corresponds to turning points of the central density. Solid line corresponds to density profiles obtained in TDHF calculation using a soft EOS. Dashed lines corresponds to fit obtained with two wood-saxon (see text).

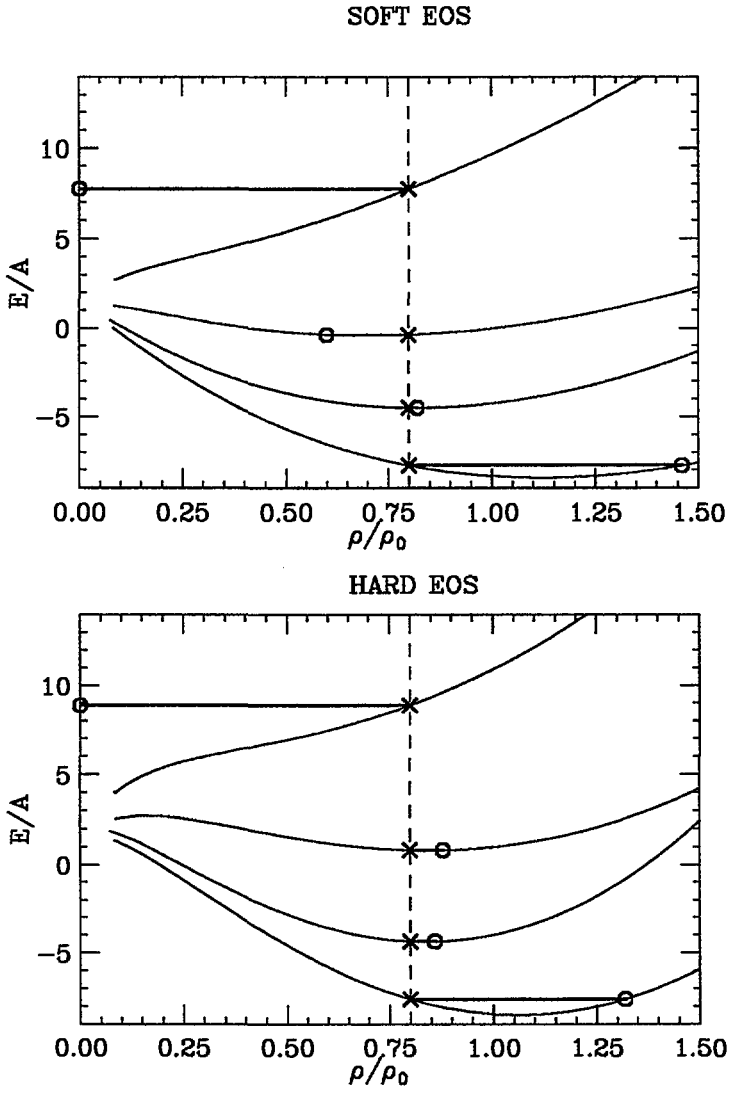

Figure 6: Shematic construction of the collective turning point using the isentropic curve in the excitation energy versus density plot, asking for both a conservation of the excitation energy and the entropy. Initial conditions are reported as crosses whereas first turning points are denoted by circles.

table 4 and figure 4, several comments should be made:

- i) For high excitation energies (small masses), the schematic construction based on energy and entropy conservation predicts a total vaporization of the nucleus whereas in the dynamical simulations a small residue survives. This discrepancy can be accounted for by considering the energy and entropy variation due to the evaporation of particles (see fig. 3).

- ii) for low excitation energy (for example $A = 191$), evaporation is negligeable (S=cte, T=cte (fig. (3)) and the result could be directly compared to the schematic construction. However, we observe that TDHF predictions differ from schematic predictions. In the schematic model, from figure 6, starting with a nucleus of mass $A = 191$ at $\eta = 0.8$, it appears impossible to reach a dilution lower than the initial one since the diluted nucleus is predicted to undergo a compression right after the beginning of the calculation. In TDHF simulations, the system is able to reach lower densities than the initial one by creating a hole at the center of the nucleus. Moreover, instead of undergoing damped monopolar oscillations, the nucleus reaches a much lower value of central density at the second dilatation[7].

In conclusion of this section, the turning point prediction of TDHF dynamics seems to show that neither at moderate nor at high energy we are able to reproduce the prediction of [4]. In particular, for initial temperature inferior to 5 MeV, the TDHF expansion does not correspond to the breathing mode picture. In this picture, the central density is taken to be the only relevant variable since a self similar expansion is explicitly assumed. In fig. 5. we show a typical example of density profile for different time of the evolution for $A = 191$. From this picture, it is clear that hollow structures are created during the evolution and that one density profile at a given time could not be obtained from another one by a simple scaling. The existence of exotic shapes which are created during the expansion, was already suggested in several works [7]. The main novelty found here as we will see, is that these structures are consequences of the beating of intrinsic collective modes[10].

[7]Note that, this effect is not due to the coulomb interaction and so is not analogous to the phenomenon reported by Borderie *et* al in ref. [7], since removing the coulomb potential from our simulations do not modify the observed behavior.

In order to get a deeper insight in the collective dynamics, we will focus on the collective dynamics in the following[8].

4.3 Collective dynamics

In this section, we have generalized the analysis performed in ref.[10] to many different initial conditions. In TDHF calculation, no assumption is made on which collective degrees of freedom could develop during the evolution.

In order to better understand the complex dynamics of the density $\rho(r,t)$, we have plotted in the fig.7 its Fourier transform $\rho(r,\omega)$ performed over 1500 fm/c. In this figure, from top to bottom, we display three different initial compression factors $\eta = 0.8, 1.0$ and 1.2. As expected, a vibration at energy $E = 12.5MeV$ is present both in $\rho(r,\omega)$ This corresponds to the expected breathing vibration and indeed the radial dependence of the density variation $\rho(r,\omega)$ is well fitted by the usual Tassie transition density[12].

In fig.7, we observe several other collective higher at higher energies. For $\eta = 0.8$, we have many additional waves at frequencies 17, 20, 25 and around $40MeV$. The collective motion located at $2 * 12.5 \simeq 25MeV$ corresponds to the two-phonon excitation of the breathing mode vibration. The other peaks at 17, 20 and around $40MeV$ could be associated to other collective degrees of freedom.

In order to study either a possible anharmonicity or a coupling between modes, we have investigate the role of the vibration amplitude changing the initial conditions. In a pure harmonic picture, frequencies should remain constant and amplitudes of responses should vary linearly with the initial perturbation. Focussing on the middle and bottom part of fig. 7, we see first that the frequencies are almost constant but the amplitude of the response do not depend linearly on the initial perturbation. Therefore, the nuclei presents non-linearities and mode couplings but they are not strong enough to destroy the collective motions. This means that we are still far from a chaotic regime.

In this chapter, we have pointed out that not only the breathing mode is excited in our TDHF calculation but also other modes. These modes are highly non-local in r. This induces a complex dynamics and in particular

[8]In the rest of the paper, we will discuss only the soft-EOS since the effect we are discussing here are generic and, from the qualitative point of view, do not depend upon the compressibility of the force used in the simulation (see fig. 4).

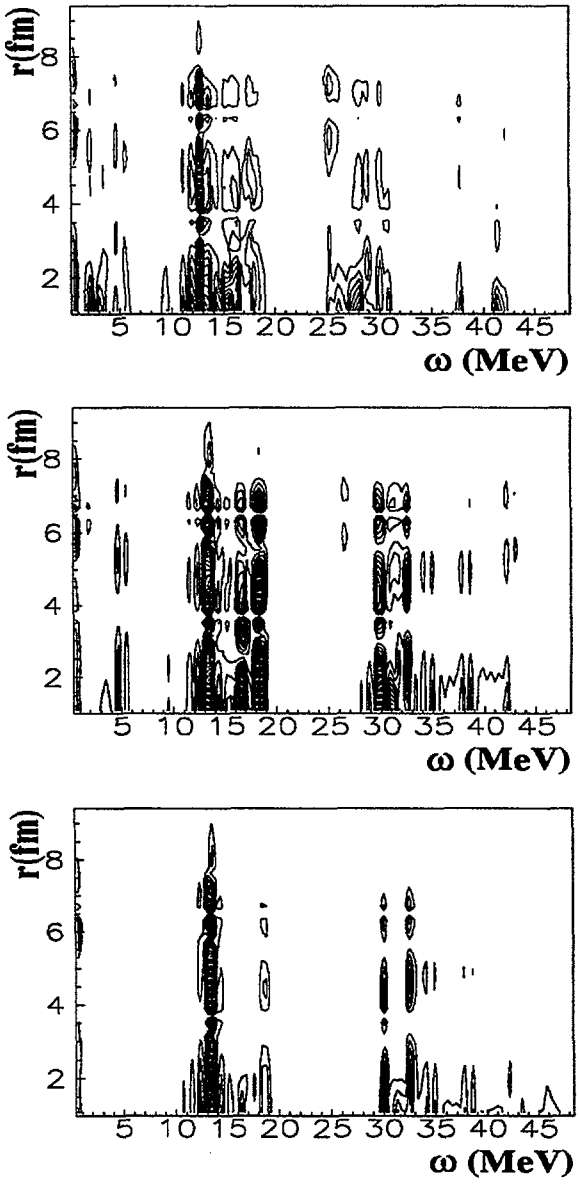

Figure 7: Fourier transform $\rho(r,\omega)$ (Left) $\rho(r,t)$. From top to bottom three different initial compression/dilatation factor are considered: $\eta = 0.8, 1.0$ and 1.2 for a nucleus of mass $A = 191$.

may lead to the creation of hollow structure. Up to now, many different macroscopic models[3, 4, 9] have been used in order to extract information about the break-up of highly excited nuclear systems. In these approaches, the breathing vibration is taken to be dominant and the expansion is assumed to be a time-dependent self-similar expansion of the nucleus. However, this picture fails to reproduce our calculation which indicate that we must extend our collective phase space to include more degrees of freedom. In the next chapter, we will address this question and illustrate a possible generalization the EOS of a finite nucleus in order to include hollow structures.

5 Inclusion of Hollow shapes of the nucleus.

During the evolution, we have seen that the nucleus could reach low density region by creating a hole at its center. In order to study this type of shape, we have parametrize the density profile as follow:

$$\rho(r,t) = \mathcal{A}\left(\frac{\rho_1 \cdot \alpha(t)^3}{1+\exp\left(\frac{r\cdot\alpha(t)-R_1}{a_1}\right)} + \frac{\rho_2/\beta(t)^3}{1+\exp\left(\frac{r/\beta(t)-R_2}{a_2}\right)}\right) \tag{21}$$

In this expression, $\mathcal{A}$ is fixed in order to conserve the number of particles. The coefficients ρ_i, R_i and a_i are fixed by fitting the density obtained during the evolution of the nucleus $A = 191$ at time $t = 108 fm/c$ (see figure 5). ρ_1, R_1 and a_1 are respectively equal to $0.0826 fm^{-3}$, $3.09 fm$ and $0.598 fm$ whereas ρ_2, R_2 and a_2 are equal to $0.1354 fm^{-3}$, $6.98 fm$ and $0.528 fm$. With this parametrization, the information contained in the density profile is now reduced to only two coefficients $\alpha(t)$ and $\beta(t)$. If $\alpha(t)$ is less than zero, the nucleus presents a hole at its center, otherwise, it presents a bump. Since ρ_2 is much bigger than ρ_1, for low values of α, the parameter β could be approximatively seen as a global scaling of the nucleus ($\beta > 1$ corresponds to a dilatation whereas $\beta < 1$ is a compression).

In figure 5, we have traced results of the best fit we have obtained for the different density displayed. Values of α and β are reported in table 5. We can see that this parametrization seems to be particularly suitable and represents well the different density profiles, so that the time dependent evolution could be accuratly replaced by the evolution of the two parameters α and β. Since we now include a more general class of density shape, this phase-space is a generalized approach of the breathing mode picture, the two variables being now interpreted as two collective coordinates.

t (fm/c)	$\alpha(t)$	$\beta(t)$
0	0.60	1.07
18	-0.80	0.98
45	0.76	0.89
108	-1.00	1.00

Table 5: Different values of $\alpha(t)$ and $\beta(t)$ obtained by fitting the density profile at divers time of the expansion of the nucleus $A = 191$.

5.1 Generalization of the zero temperature equation of state.

Using the parametrization (21) we can define the EOS in the (α, β) phase space by computing the energy at zero temperature for different α and β parameters. Since eq. (21) defines only the density profile and not the wave-functions, we have used the Extended Thomas Fermi formalism described in [15] where two additional terms are added to the usual Thomas Fermi kinetic energy

$$E_K(r) = E_{TF}(r) + \frac{\hbar^2}{2m}\left(\frac{1}{36}\frac{(\nabla\rho(r))^2}{\rho(r)} + \frac{1}{3}\Delta\rho(r)\right) \tag{22}$$

In this expression, E_{TF} take the form (12). The total energy is calculated by incorporating the potential (2) and integrating over the r-space.

By varying the parameters, we can have the generalized EOS: $E = E(\alpha, \beta)$. This EOS is represented in fig.8. The graphic of a self-similar picture displayed in figure 6 for $A = 191$ could be recovered by cutting the graphic with a surface $\alpha = f(\beta)$ (which could be roughly approximated by $\alpha \simeq cte$. In this picture, we can see different potential wells with different minima with almost degenerated energies separated by small barriers (of the order of $1-2$ MeV). These three minima correspond respectively to a nucleus with a hole ($\alpha < 0$), a standard Wood-Saxon shape ($\alpha = 0$) and a nucleus with a bump at the center ($\alpha > 0$).

In order to study the evolution of the system in this $E(\alpha, \beta)$ phase-space, we have performed a fit of the density profile at each time. Results is shown up to $108 fm/c$ in figure 9. The path in this phase-space appears complex and cannot be reduced to a scaling of the β variable. This is another indication of the fact that we cannot reduce the TDHF dynamics to a breathing mode

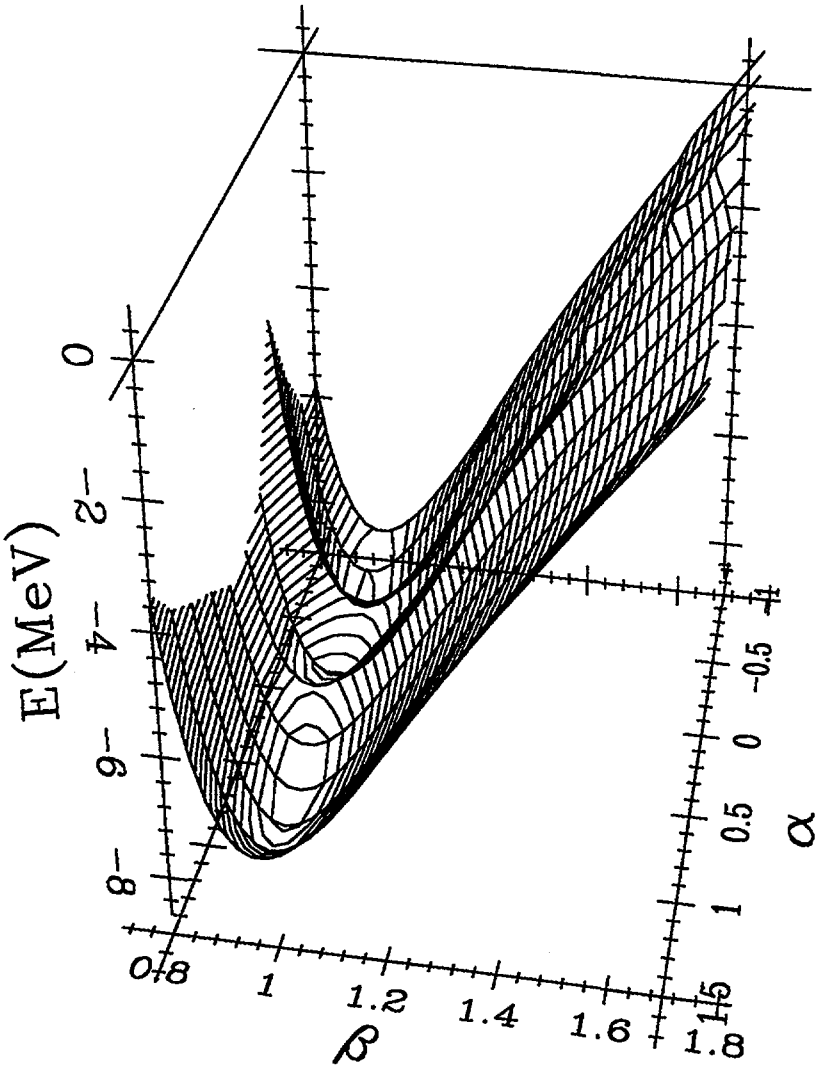

Figure 8: Representation of a generalised EOS which include hollow structures. The energy is reported as a function of α and β. α greater than 0 corresponds to nucleus with a bump whereas α less than one corresponds to a nucleus with a hole at its center. On the other side, $\beta > 1$ is equivalent to a compression and $\beta < 1$ means a dilatation.

picture. During the evolution, we see that the nucleus could go in many different configurations in this phase space.

In summary, the dynamical expansion as the one studied by [4] is only justified if we assume a strong predominance of the breathing mode. In a microscopic calculation, other collective vibrations can be excited during the dynamical evolution. This lead to a complex dynamics for hot and compressed (or dilated) systems for moderate energies. As a direct consequence, the dynamics should be discussed in an enlarged phase-space of several collective degrees-of-freedom. The illustrative pictures (8 and 9) seems to indicate that energetically hollow and uniform nuclei should be both taken into account on the same level. Note however, that for initial temperature greater than 5 MeV, many orbitals are occupied and levels crossing seems less important and we do not observe this effect anymore.

Finally, we want to mention that the theoretical determination of an effective temperature during the evolution of the expanding source, is often a hard task and is often not possible since the system is only equilibrated at the initial time. During the dynamics, the nucleus is strongly out-of equilibrium and no energy and occupations numbers of levels could be defined on the same time (no approximative Fermi-Dirac distribution could be defined [9]). However, we can imagine another way of defining the temperature. Indeed, it is possible to follow the density and the energy of the excited system with time. In a breathing mode picture, we have a univocal correpondance between these two parameters and the temperature: i.e. the EOS $E = E(\rho, T)$. However, this picture breaks in our calculation since we have to consider at least $E = E(\alpha, \beta, T)$ and in fact two parameters are often not enough. In conclusion, the determination of an effective temperature in models as the one we are considering, is not well-defined as far as no equilibration process is added on top of the mean-field.

6 Discussion

We have used a quantum microscopic simulation in order to test the interpretation of the caloric curve recently proposed by Papp and Nörenberg[4]. In their work the experimentally observed caloric curve could be interpreted as a line of turning-point reached in the low density region during the monopole

[9]Indeed, during the evolution the Hamiltonian $\hat{h}$ and the density $\hat{\rho}$.

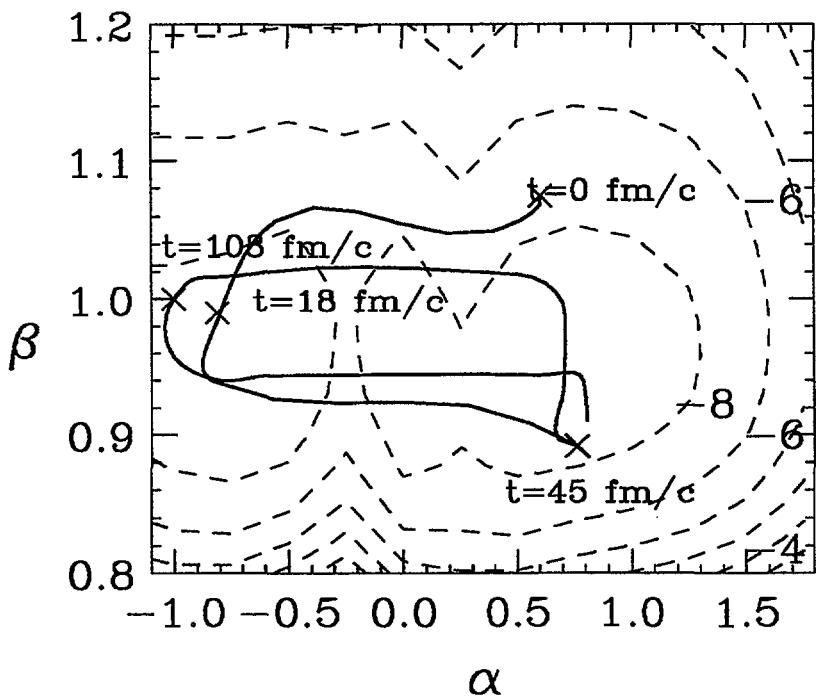

Figure 9: Dynamical Path of TDHF simulation in the (α, β) phase-space. Contour plot (dashed lines) of the energy are also displayed (contour corresponds to $-8, -7, -6, -5$ and $-4MeV$.

expansion of excited nuclei where the nucleus could break. Using analogous initial conditions, we have pointed out that many differences between a microscopic approach and the collective model. Indeed at low and moderate energies, the TDHF dynamics indicate that different collective vibrations could develop on top of the self-similar vibration. This collective behavior may lead to the formation of hollow structures. Since the density come from a superposition of many modes, we see that the lowest density region could be reached after a longer time (see fig. 4) than the first breathing of the nucleus. It should be noticed that experimental DATA of photon detection seems to indicate such a behavior[20]. The presence of many collective mode in the dynamic has led us to generalize the simple breathing mode picture. By a suitable parametrization of the density, we have defined a generalized Equation Of State. This new approach, include the possible existence of exotic shape in the dynamic. As we have seen, the nucleus has a complex path in this new phase-space. On the other hand, at high initial excitation energy, when the breathing collective mode dominates, the amplitude of the monopole oscillation again do not corresponds to those predicted in [4]. As a direct consequence, our simulations do not confirm the interpretation of the caloric curve based on a self-similar expansion of the abraded nuclei.

7 Acknowledgements

We thank J.P. Wieleczko and A. Chbihi for helpfull discussion on the manuscript.

References

[1] J. Pochodzalla *et al*, Phys. Rev. Lett. **75** (1995) 1040.

[2] Y.-G. Ma *et al*, Phys. Lett. **B390** (1997) 41.

[3] J. Pochodzalla *et al*, Critical Phenomena and collective observables (CRIS96), Acicastello, Italy, May 27-31, 1996, Ed. S. Costa *et al*, p.1.

[4] G. Papp and W. Nörenberg, International Workshop XXII on Gross Properties and Nuclear Excitation, Hirschegg, Austria, January, 17-22, 1994, p. 87. G. Papp and W. Nörenberg, Critical Phenomena and collective observables (CRIS96), Acicastello, Italy, May 27-31, 1996, Ed. S. Costa *et al*, p.377.

[5] J. Pochodzalla, Prog. Part. Nucl. Phys. **39** (1997) 443.

[6] D. Lacroix and Ph. Chomaz; Preprint GANIL 98-04

[7] W.Bauer *et al*, Phys. Rev. Lett. **69** (1992) 1988.
L.G.Moretto and G.J. Wozniak, Ann. Rev. Nucl. Part. Sc. **43** (1993) 379.
B. Borderie *et al*, Phys. Lett. **B302** (1993) 15.

[8] D. Vautherin, J. Treiner and M. Veneroni, Phys. Lett. **B191** (1987) 6.

[9] G. Bertsch and P.J. Siemens, Phys. Lett. **126B** (1983) 9. J. Cugnon, Phys. Lett. **135B** (1986) 374.(*and ref. therein.*) W. A. Friedman, Phys. Rev. Lett. **60** (1988) 2125. W. A. Friedman, Phys. Rev. **C 42** (1990) 667.

[10] D. Lacroix and P. Chomaz; Preprint GANIL 97-35.

[11] J.-J. Gaimard and K.-H. Schmidt, Nucl. Phys. **A531** (1991) 709.

[12] P. Ring and P. Schuck, *The Nuclear Many-Body Problem, Spring-Verlag*, New-York (1980).

[13] D. Vautherin, J. Treiner and M. Veneroni, Phys. Lett. **B191** (1987) 6.

[14] S.E. Koonin and J.W. Negele, Phys. Rev. **C15** (1977) 1359. K.T.R. Davies and S.E. Koonin, Phys. Rev. **C23** (1981) 2042.

[15] M. Brack, C. Guet and H. Håkansson, Phys. Rep. **5** (1985) 275.

[16] P. Bonche, S. Koonin and J.W. Negele, Phys. Rec. **C13** (1976) 1226.

[17] G.F. Bertsch and S. Das Gupta, Phys. Rep. **160** (1988) 189.

[18] Ph. Chomaz, N. Van Giai and S. Stringari, Phys. Lett. **B189** (1987) 375.
N. Van Giai *et al*, Nucl. Phys. **A482** (1988) 437c.

[19] W.A. Friedman, *8-th Winter workshop on Nuclear Dynamics, Jackson Hole, Wyoming, 1992.*

[20] For a review, see Y. Schutz *et al*, Nucl. Phys. **A622** (1997) 404.